FULL ARTICLE

Light distribution and thermal effects in the rat brain under optogenetic stimulation

*Barbara Gysbrechts**, 1, *Ling Wang*[1], *Nghia Nguyen Do Trong*[2], *Henrique Cabral*[3], *Zaneta Navratilova*[3], *Francesco Battaglia*[3], *Wouter Saeys*[2], and *Carmen Bartic*[1]

[1] Department of Physics and Astronomy, University of Leuven, Celestijnenlaan 200D, 3001 Leuven (Belgium)
[2] Department of Biosystems, University of Leuven, Kasteelpark Arenberg 30, 3001 Leuven (Belgium)
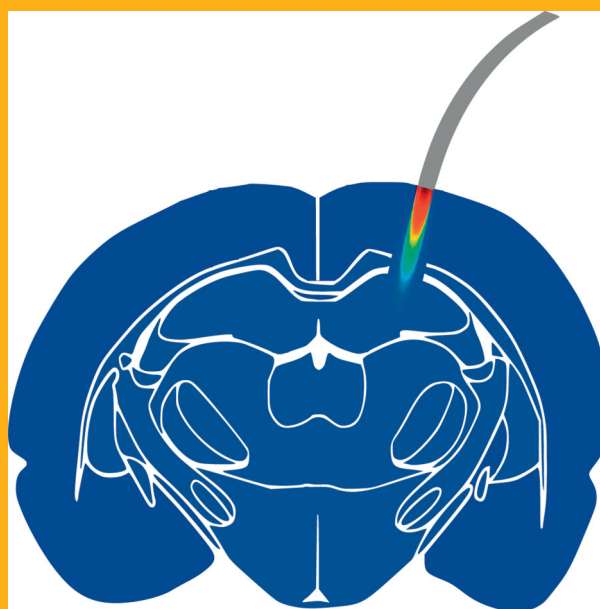[3] Donders Institute, Radboud University, Heyendaalseweg 135, 6525 AJ Nijmegen (The Netherlands)

Optical brain stimulation gained a lot of attention in neuroscience due to its superior cell-type specificity. In the design of illumination strategies, predicting the light propagation in a specific tissue is essential and requires knowledge of the optical properties of that tissue. We present the estimated absorption and reduced scattering in rodent brain tissue using non-destructive contact spatially resolved spectroscopy (cSRS). The obtained absorption and scattering in the cortex, hippocampus and striatum are similar, but lower than in the thalamus, leading to a less deep but broader light penetration profile in the thalamus. Next, the light distribution was investigated for different stimulation protocols relevant for fiber-optic based optogenetic experiments, using Monte Carlo simulation. A protocol specific analysis is proposed to evaluate the potential of thermally induced side effects.

1. Introduction

In the past decade, the use of photonic methods in neuroscience increased tremendously. Understanding the function of neural circuits requires tools to record, but also to selectively perturb the activity of cells in a given circuit. Since 2005 a large number of light-sensitive proteins have been expressed into mammalian neurons that allow cellular activation or inhibition of cells exposed to visible light illumination [1]. As a perturbation technique, light-induced stimulation has several advantages over electrical techniques, such as better spatial control of the stimulated area, no electrical artifacts, minimized tissue

* Corresponding author: e-mail: barbara.gysbrechts@fys.kuleuven.be, Phone: +32 16 322 672

damage, and cell type specificity. Optogenetics is currently one of the most popular techniques in neuroscience, thanks to its flexibility. Opsins, the protein responsible for converting light energy into electrical energy that generates or blocks action potentials, have been designed for functionality in the targeted cell type, speed, and their wavelength sensitivity [1].

Since too high light intensities can cause brain damage, while too low intensities may be insufficient to activate or inhibit neural activity, a well-designed stimulation protocol is required. In *in vivo* optogenetic experiments, optic fibers are usually inserted into the brain to access the regions of interest. Recently, the use of fiber optics has been explored for simultaneous control and measurement of neural activity [2], and for stimulation of multiple brain regions along the fiber [3]. However, in most of the studies, fairly large brain regions are illuminated by multi-mode optic fibers (common core diameter values are 100 and 200 μm) while the cell-type selectivity should only occur from the genetic targeting of specific cell types with opsins. Since genetic targeting is never 100% specific and because one should avoid unnecessary tissue exposure to light, methods that allow tissue illumination with high spatial resolution are highly desirable [4–6].

The light intensity profile generated by an optic fiber in a tissue is determined by the source power, the fiber's numerical aperture, NA, the core diameter, d_{core}, and the wavelength dependent optical properties of the tissue (absorption coefficient, μ_a, scattering coefficient, μ_s, refractive index, n, and anisotropy factor, g). Prediction of the light profile is valuable in defining a suitable protocol for a specific optogenetic experiment. Whereas knowledge of the tissue's optical properties is required for this purpose, reported values in literature are rare, especially in the visible spectrum for small animals such as mice and rats.

To measure the optical properties of brain tissue, the integrating sphere method incorporating the adding-doubling algorithm is frequently used [7–10]. While this method is widely used, brain tissue must be sliced in order to measure reflectance and transmittance separately. However, because each of the tissue preparation steps (fixation, embedding, sectioning) can lead to shrinkage, swelling, or deformation of the brain, it would be useful to find a less invasive approach for measurement of optical properties [11]. Moreover, the optical properties have often been determined only at one wavelength per measurement [10, 12].

In this study, we measured the optical coefficients of different tissue structures in rat brain and investigated light propagation and caused thermal effects in the brain as a function of external properties such as fiber diameter, aperture, power, and wavelength. These physical characteristics are of high concern in optogenetic experiments. Contact spatially resolved spectroscopy (cSRS) was employed to estimate the optical properties of the cortex, hippocampus, striatum, and thalamus of the rat brain over a broad wavelength region ranging from 470 nm to 1040 nm. The optical absorption coefficient μ_a and reduced scattering coefficient $\mu'_s = \mu_s (1 - g)$ were estimated from the recorded spatially resolved reflectance intensity profiles. Based on the obtained optical properties, irradiance profiles in the brain tissue were modeled and discussed for fibers with different NA and d_{core}, and for different wavelengths and light source powers. The shape and volume of perturbed neurons was investigated as a function of these parameters, assuming a lower threshold for opsin activation of 1 mW/mm^2 [13, 14]. Finally, the potential of heat-induced cell damaging effects was investigated by calculating transient temperature changes during pulsed light stimulation. Heat-induced damage and phototoxic effects caused by the increase in oxidative stress of the illuminated cells, both leading to altered cell behavior and cell viability [28], are reduced when the light intensity and exposure time are limited.

2. Materials and methods

2.1 Animal subjects

Ten adult Long Evans rats were deeply anesthetized with an overdose of pentobarbital. Immediately after extraction, the brains were kept in saline solution at 4 °C until the measurements were performed. The use of animals and procedures was approved by the Ethical Committee for Animal Welfare of the University of Leuven.

2.2 Spatially resolved spectroscopy

The custom built spatially resolved spectroscopy instrument described in [15] was used to estimate the wavelength dependent absorption, μ_a, and reduced scattering coefficients, $\mu'_s = \mu_s(1 - g)$, of rat brain tissue for the spectral range between 470 nm and 1040 nm, relevant for optogenetic experiments. Briefly, the set-up consists of a custom fiber-optic probe with one source fiber emitting the light, and five fibers collecting the reflected light at distinct distances from the source. The collected light is then sent to a spectrograph and the spatially resolved diffuse reflectance is acquired as function of wavelength (Figure 1). A metamodel trained on measurements acquired for a set of liquid phantoms covering a wide range of known optical properties was used to extract the μ_a and μ'_s val-
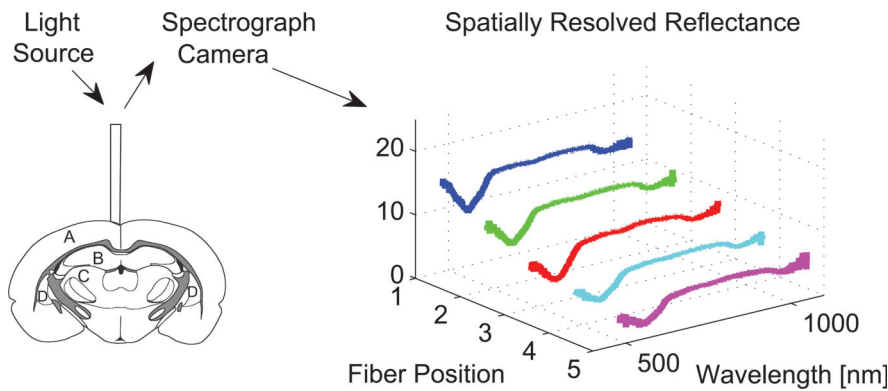
Figure 1 Working principle of contact spatially resolved spectroscopy. A fiber bundle consisting of six fibers with 200 μm diameter and 0.22 numerical aperture was used to illuminate the sample and to collect the reflected light at five distances from the source fiber, ranging between 0.3 mm and 1.2 mm (left). The collected light was sent to a spectrograph and camera, resulting in spatially resolved reflectance profiles in the 470–1040 nm wavelength range (right).

ues from the collected reflectance profiles, described in detail in our previous publication [16].

The measurements were performed *in vitro* on the cortex (A), hippocampus (B), thalamus (C), and striatum (D), Figure 1. In order to reach the structures below the brain surface (B, C, D), the cortex (and subsequently the hippocampus) was cut in the posterior-anterior direction and turned over using tweezers until the desired region became accessible.

For each brain structure, three locations separated by at least 1.9 mm (probe diameter) were randomly selected. At every location, five cSRS measurements were repeated. The acquisition time for a single measurement at one selected location was 140 ms and the time interval between two consecutive repeated measurements was less than 1 s. All measurements on one structure were performed within 1 minute. The five repeated measurements obtained at a location on a structure were averaged in order to reduce noise effects during measurements and the averaged data were then used for estimating the optical properties (μ_a and μ'_s) spectra at that location. This procedure was applied on ten different brains for the cortex, and on seven brains for all other structures. Finally, μ_a and μ'_s spectra for each structure were obtained by averaging the results over all the measured locations of all the brains. All measurements were performed in a dark room, within 4 h after brain extraction.

2.3 Light distribution in rat brain tissue

Light irradiance distribution in brain tissue was investigated by using a 3D Monte Carlo model for steady state light transport in multi-layered tissue [17, 18], with the tissue optical properties estimated by the cSRS method and the parameters of the light source as input parameters. The refractive index for all simulations was set to 1.4 [19]. In each simulation,

5 million photons were launched uniformly across the entire fiber core surface and over a range of angles within the cone defined by the NA of the excitation fiber. The rules of photon propagation are expressed as probability functions that describe the step size of the photon movement between sites of photon-tissue interaction, and the scattering angle of a photon on its trajectory. The output of the simulation is the irradiance, I, as a function of the radial and axial distance to the source.

2.4 Thermal effects on the rat brain during pulsed light stimulation

The temperature at the fiber tip in the brain tissue was calculated as a function of time for stimulation protocols with different power, laser pulse length t_L, and frequencies. The temperature increase generated by a single pulse ΔT_1 was calculated using

$$Q = C\rho\,\Delta T_1 \tag{1}$$

with Q the absorbed energy per volume: $I \times t_L \times \mu_a$ (I at tissue-light source contact surface), C the specific heat of the brain tissue: 3650 mJ/(g · K), and ρ the brain tissue density: 1040 kg/m^3 [20]. This is valid when t_L is much shorter than the thermal relaxation time t_R, and sets the upper limit of ΔT_1 since heat conduction during the pulse is neglected [21].

The temperature decrease due to conduction after a pulse was obtained using the exponential decay law [22]

$$T(t) = T_0 + \Delta T\,\mathrm{e}^{-\frac{t}{t_R}} \tag{2}$$

with T_0 = 37 °C the initial brain temperature. For continuous pulsed stimulations, all contributions to T were summed.

Since part of the energy is used to initiate the optogenetic photocycle, the assumption that the absorbed energy is completely converted into heat results in a maximal temperature increase estimate.

3. Results and discussion

3.1 Optical properties of fresh rat brain tissue

The absorption and reduced scattering coefficients, μ_a and μ'_s, for the cortex, hippocampus, striatum, and thalamus were estimated using contact spatially resolved spectroscopy. Stability of these optical properties was proven for at least 4 hours after brain extraction [26].

The absorption and reduced scattering coefficients for the hippocampus, averaged over all the measured locations of the seven brains, are shown in Figure 2 for wavelengths between 470 nm and 1040 nm. The dotted lines represent the average value ± one standard deviation. A strong peak in absorption coefficient is observed around 550 nm, generated by remaining hemoglobin molecules (Hb). Since [Hb] depends strongly on the position in the brain and on the sample treatment, the standard deviation is the largest at this absorption maximum. The increase in absorption at wavelengths higher

than 900 nm is related to absorption by water molecules (peak at 970 nm).

The reduced scattering coefficient decreases with increasing wavelength in accordance with the Rayleigh scattering theory, typically dominant for wavelengths below 500–600 nm, and Mie scattering theory, dominant above 500–600 nm [27]. The two valleys around 585 nm and 990 nm could be explained by the limitation of the inverse metamodeling method to estimate μ_a and μ'_s fully independent of each other when μ_a becomes large relative to μ'_s.

The results for the estimated μ_a and μ'_s in all measured regions are shown in Figure 3. One can see that the optical properties for the hippocampus, striatum, and cortex are similar to each other, but lower than for the thalamus. The absorption coefficient and reduced scattering coefficient values for the cortex are at least 1.4 times smaller compared to the thalamus values, respectively in the 470–600 nm range and in the whole spectrum (470–1040 nm).

As a consequence, light penetrates deeper in the cortex, hippocampus, and striatum, but the light profile is narrower when compared to the light profile in the thalamus. This was confirmed by performing irradiance distribution simulations for both tissues. Earlier work showed that the thalamus had higher μ_a and μ'_s than native grey matter in human brain [8]. Since white matter has significantly higher optical coefficients [8, 28], we can hypothesize that the internal capsule (white matter) surrounding approxi-
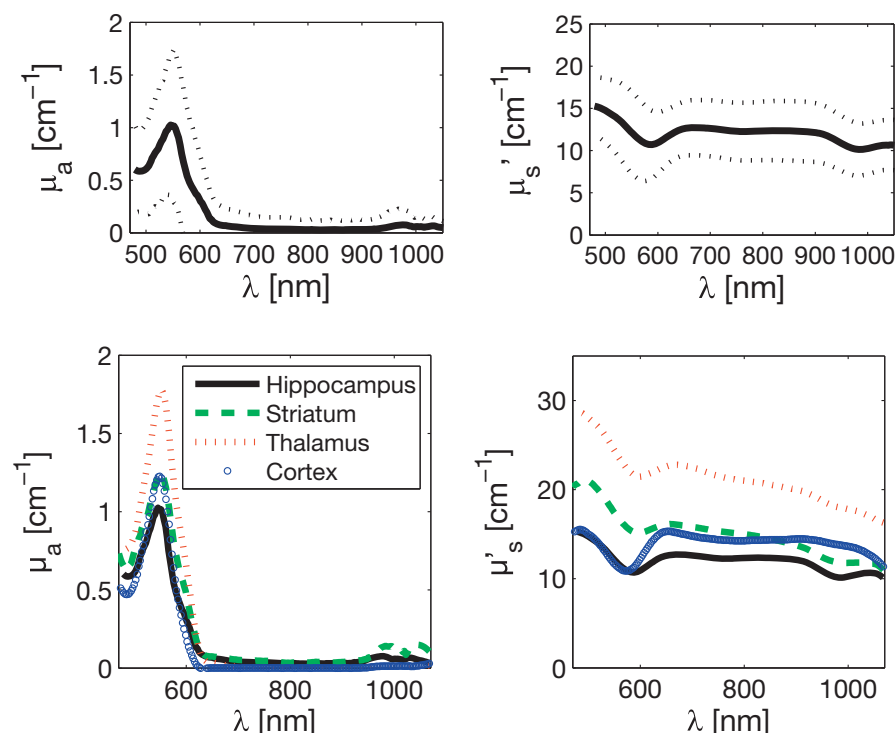

Figure 2 Absorption (left-panel) and reduced scattering (right-panel) coefficients for the rat hippocampus measured by contact spatially resolved spectroscopy on fresh tissue. The dotted lines represent the average value ± one standard deviation.

Figure 3 Absorption and reduced scattering coefficient for the rat hippocampus (black), striatum (dashed), thalamus (dotted), and cortex (circles). The thalamus has higher absorption and reduced scattering coefficients than the other investigated brain regions.

mately half of the thalamus, contributes to an increase in its estimated absorption and reduced scattering coefficients. Finally, angiograms giving details on blood volume distribution and blood flow in the different brain structures *in vivo* would be helpful in explaining the measured difference.

3.2 Review of the data on optical properties of the cortex

The experimentally obtained μ_a and μ'_s values for the cortex in the wavelength range 470–700 nm are shown in Figure 4 together with values obtained in previous studies by the integrating sphere method for human [7, 8] and rat [9, 10] brain tissue. Whereas in most cases the μ_a and μ'_s values follow the same trend, relatively large variations in data amongst the different publications can be observed. The μ_a and μ'_s values obtained in this work are similar to the values for native gray matter in human brain measured by using the integrating sphere method [8]. As in our study, the brain was not included in agar before performing the measurement. It would be interesting to make a comparison between results obtained from different approaches. However, there is still a lack of data in literature for the optical coefficients in the different regions in rat brain.

The main absorbing component in this wavelength range is hemoglobin, causing a peak in μ_a at around 560 nm [29]. The residual blood content and hence hemoglobin concentration in the sample strongly depends on the tissue preparation procedure, resulting in difficulties in comparison. Moreover, tissue preparation also influences the reduced scattering coefficient. In this work, the sample was fresh (<4 h), not perfused, and not included in agar.

Except for our data, all the data sets shown in Figure 4 were obtained by the integrating sphere method on sliced tissue. This tissue preparation method leads to changes in cell size, distribution and drying at the cut surface that may significantly influence the values of the optical parameters [11].
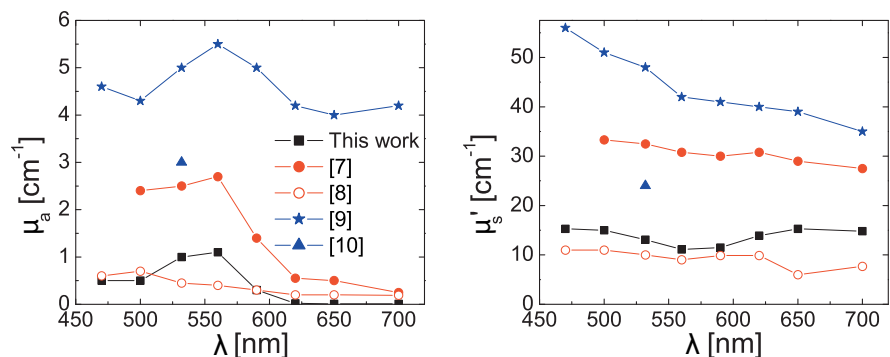
3.3 Light distribution in rat brain for a variety of light sources

A Monte Carlo algorithm was used to study the influence of numerical aperture, fiber diameter, wavelength, and power on the light intensity distribution (irradiance profile) in the rat brain. From the perspective of optogenetic experiments, a comparison was made between illuminated tissue volumes for different optical configurations, assuming that 1 mW/mm² is the irradiance threshold for opsin stimulation [30]. Since the focus of this study is characterizing the influence of external parameters on the shape and volume size of stimulated neurons, the light propagation modeling was limited to an infinitely wide homogeneous tissue with a sufficient thickness and optical coefficients were those obtained for the cortex. The volume of stimulated neurons was calculated assuming rotational symmetry around the z-axis (depth) of the obtained irradiance profile. In previously reported studies, the measured value of refractive index of tissue varies between 1.38 and 1.41 [31, 32]. Changing the index value between these values brings a maximal deviation in the calculated volume of 1% that is negligible.

3.3.1 Influence of numerical aperture and fiber diameter on light distribution

The influence of NA on the irradiance distribution was studied by calculating irradiance profiles for optical fibers with core diameters between 9 μm and 200 μm, and NA's equal to 0, 0.12, and 0.37 at a wavelength of 470 nm. Contour plots for irradiances of 1 mW/mm² and 5 mW/mm² are shown in Figure 5 for a fiber with 200 μm diameter (input power: 1 mW). For all investigated fiber diameters, stronger attenuation occurs in the axial direction, and weaker attenuation in the radial direction for larger numerical apertures. This effect is maximal close to the fiber tip, where the irradiance is high.

Figure 4 Absorption coefficients (left) and reduced scattering coefficients (right) of the cortex for wavelengths between 450 nm and 700 nm in rat brain (squares, triangles, asterisks) and human brain (dots, circles).
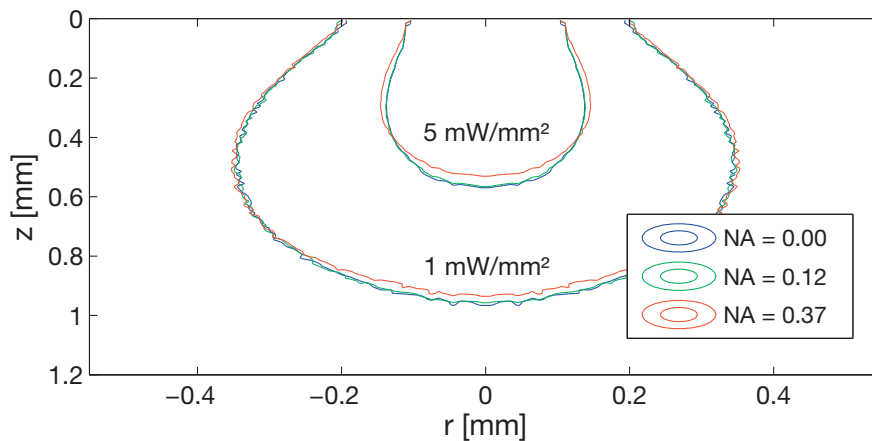
Figure 5 Contour lines at 1 mW/mm^2 and 5 mW/mm^2 for fibers with diameter 200 μm, and NA equal to 0, 0.12, and 0.37 (Power: 1 mW, wavelength: 470 nm). Close to the tip the difference in irradiance is maximal, with strongest attenuation in z-direction and weakest attenuation in r-direction for high numerical aperture fibers.

The irradiance distribution was simulated for fibers with NA = 0.37, and core diameters of 50 μm, 100 μm, and 200 μm. The resulting contour plots for 1 mW/mm^2 and 5 mW/mm^2 are shown in Figure 6 (input power: 1mW). Optical fibers with larger core diameters have higher attenuation in the axial direction and lower attenuation in the radial direction. Again, this effect is largest close to the fiber tip.

The volume of stimulated tissue was calculated for all configurations and a maximal volume increase of 5% was observed going from lowest NA to highest NA, or from smallest diameter to largest diameter.

Finally, contour lines were calculated for the stimulation protocols used in [33] (200 μm, 2.5 mW, 473 nm) and [34] (10 μm and 200 μm, 1 mW, 473 nm). In both cases the reported contour lines overlap with ours within ~40 μm accuracy.

3.3.2 Influence of wavelength on the intensity profile

Intensity profiles were simulated for a typical multi mode (MM) fiber (NA = 0.37 ± 0.02, d = (200 ±

8 μm) and a single mode (SM) fiber (NA = 0.12 ± 0.01, d = (9 ± 1.5) μm) for wavelengths between 470 nm and 1040 nm. The corresponding stimulated volumes were calculated from these profiles, using 1 mW as input power. As shown in Figure 7, both types of fibers follow the same trend with a minimal stimulation volume around 550 nm caused by the absorption maximum. As predicted by the results in the previous section, the MM fiber stimulates a larger volume of neurons compared to the SM fiber, with a maximal relative difference of 6%.

3.3.3 Influence of the power on the stimulation volume

The power of the light source needs to be carefully selected since it determines the range in which opsins will be stimulated. An upper threshold should also be set in order to prevent phototoxic effects and overheating of the brain. Whereas at a fixed point in the tissue the irradiance increases linearly with the applied power, the volume with irradiance larger than 1 mW/mm^2 increases faster. The stimulated vol-
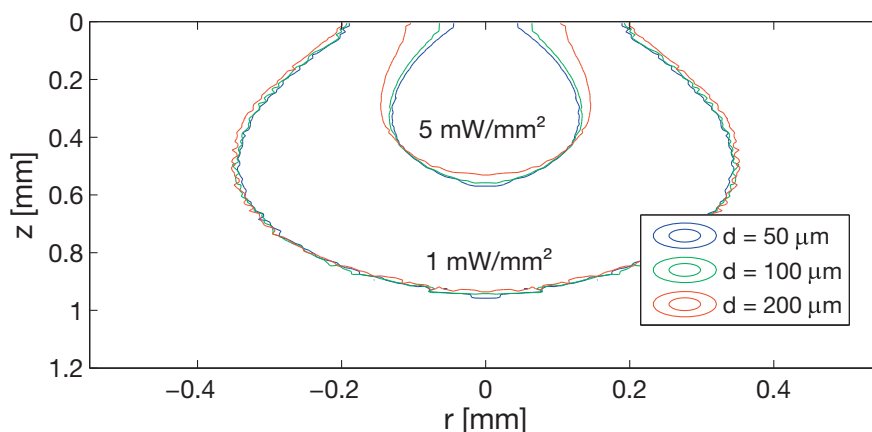

Figure 6 Contour lines at 1 mW/mm^2 and 5 mW/mm^2 for fibers with NA = 0.37, and diameters equal to 50 μm (blue), 100 μm (green), and 200 μm (red) (Power: 1 mW, wavelength: 470 nm). Close to the tip the difference in irradiance is maximal, with strongest attenuation in z-direction and weakest attenuation in r-direction for high fiber diameters.
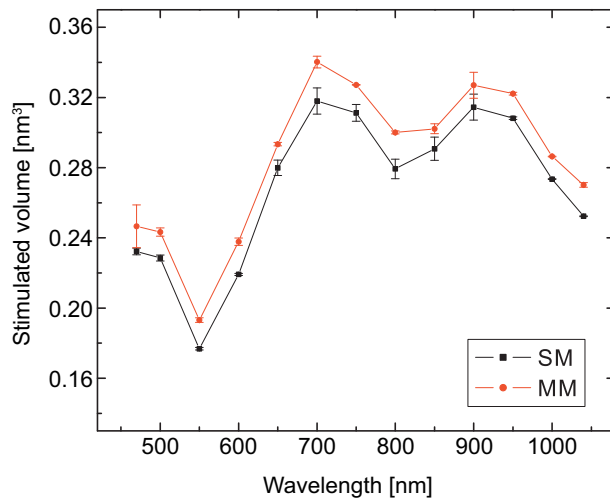
Figure 7 Volume of stimulated tissue ($I > 1$ mW/mm^2) as a function of stimulation wavelength for the same input power 1 mW. The multi mode fiber (MM, black) has significantly larger stimulation volumes then the single mode fiber (SM, red). The volume is minimal for wavelengths in which hemoglobin is absorbing light.

ume was calculated as a function of applied power and fitted for a standard multi mode fiber (NA = 0.37 ± 0.02, $d = (200 \pm 8$ μm)) and single mode fiber (NA = 0.12 ± 0.01, $d = (9 \pm 1.5$ μm)) at 470 nm, resulting in a third power dependency shown in Figure 8. On the one hand, the absolute difference between stimulation volumes for SM and MM fibers is small. On the other hand, the relative difference grows fast with decreasing power, resulting in a 7% larger V_{MM} at 5 mW, and a 17% larger (V_{MM} at

0.5 mW compared to V_{SM}. We can conclude that the influence of fiber properties on the beam profile in the tissue increases when the power is lowered.

3.3.4 Influence of irradiance on the stimulation volume

The amount of light required to excite or inhibit a region of neurons is determined by the threshold irradiance for opsin activation. From this point of view, a comparison can be made between the light profiles generated by a SM and a MM fiber with the same input *irradiance* instead of input *power*. Since much higher irradiance levels can be obtained with SM fibers as compared to MM fibers for the same input power, the excitation volume will be much smaller compared to that of a MM fiber for the same irradiance values (Figure 9). This is a very interesting feature for achieving better spatial localization of the activation when using a SM fiber.

The volumes with irradiance higher than 1 mW/mm^2 (V_{stim}) were calculated for input irradiances ranging from 1 mW/mm^2 to 100 mW/mm^2 at 470 nm, and are shown in Figure 9. Whereas V_{stim} is increasing linearly with the irradiance for a SM fiber (left axis), V_{stim} can be fitted with a quadratic function for the MM fiber (right axis). When large volumes of neurons are to be stimulated, the use of MM fibers is recommended since less irradiance and power are required compared to a SM fiber, reducing the risks for phototoxic and heat induced effects.

The maximal volume that can be stimulated with a SM fiber for a typical stimulation protocol (t_L =
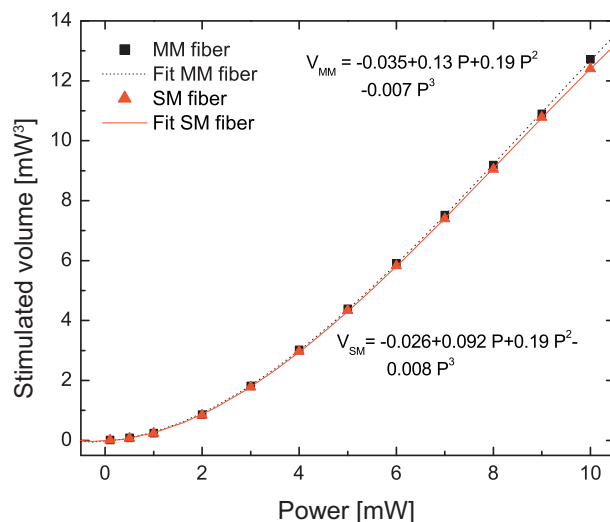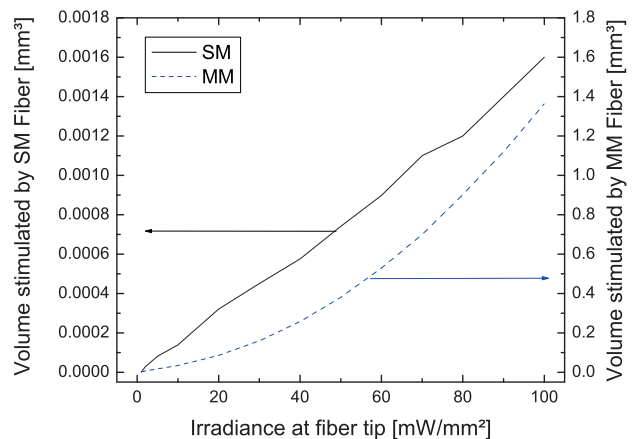

Figure 8 In the depicted input power range, a third power relationship is observed between the calculated volume of stimulated neurons and the applied power for a multi mode (black squares) and single mode (red triangles) fiber emitting light at 470 nm.

Figure 9 The calculated volume with irradiance higher than 1 mW/mm^2 for a standard SM (left axis) and MM (right axis) fiber with input irradiances at the fiber tip ranging from 1 mW/mm^2 to 100 mW/mm^2 at 470 nm. A quadratic increase in V_{stim} was observed for the MM fiber, whereas V_{stim} increases slower and linearly for the SM fiber.

Table 1 Temperature increase during pulsed stimulation of ChR2 in rodent brain ($\lambda = 470$ nm).

Irradiance [mW/mm^2]	Pulse length [ms]	Frequency [Hz]	ΔT_1 [°C]	ΔT_{sat} [°C]	Reference
70.5	5	5	0.005	0.005	[37]
		20		0.007	
		130		0.032	
380	30	5	0.153	0.156	[13]
		10		0.175	
		20		0.237	
46	1	40	0.0006	0.002	[38]
	100	(single pulse)	0.062	–	
10	4	5	0.0005	0.0005	[32]
		10		0.0006	
		45		0.001	
5	20	8	0.001	0.001	[39]

10 ms, $f = 10$ Hz) while staying below a temperature increase of 1 °C was determined using Eq. (1, 2) and the Monte Carlo model. This resulted in $V_{stim, max} = 0.001$ mm$^3 = (100$ μm$)^3$. If a larger volume of neurons needs to be stimulated, a MM fiber is recommended. Since the power equals the irradiance divided by the fiber core area, the irradiance at the fiber tip will be approximately 500 times less when switching from SM fiber ($d = 9$ μm) to MM fiber ($d = 200$ μm), keeping the same power.

When small activation volumes ($<10^{-3}$ mm or 100 μm × 100 μm × 100 μm) are desirable, the use of SM fibers is recommended when power needs to be minimized, which is of high importance in miniaturized devices with integrated light sources. If minimization of energy consumption is of minor importance, the fiber choice can depend on the shape of the targeted neuron region. For example, when $V_{stim} = 0.1 \cdot 10^{-3}$ mm^3 the ratio z_1/r_1 is 14 and 0.06 for a SM and MM fiber, respectively. Hence, SM fiber illumination might be desirable for targeting deeper brain structures and a MM fiber for wide shallow regions.

3.4 Temperature evolution during pulsed stimulation

To evaluate the presence of heat-induced effects during optogenetic stimulation, the temperature at the fiber-tissue interface was calculated as a function of time using Eq. (1, 2), with the pulse length, t_L, frequency, f, and irradiance at the fiber tip, I, as variables. The thermal relaxation time for the stimulation with a 200 μm diameter fiber in cortical tissue at 470 nm is 48 ms, taking into account axial and radial diffusion [35]. For a typical stimulation protocol used in optogenetics ($t_L = 10$ ms, $f = 10$ Hz, $I = 100$ mW/mm^2) the temperature increase caused by

absorption of photons during one pulse, ΔT_1, is 13.5 °C and initially each pulse increases the maximal temperature in the tissue. After less than a second, the temperature increase and decrease caused by consecutive light pulses become equal to each other and an equilibrium is reached. The saturation temperature T_{sat} is defined as the maximal temperature reached at equilibrium, in this case $T_{sat} = 37.02$ °C.

According to the laws of thermodynamics, ΔT_1 increases linearly with both pulse length and irradiance. The maximal temperature always saturates and increases linearly with t_L, I, and f. The temperature evolution at the fiber-brain interface was calculated for multiple stimulation protocols found in literature for ChR2 excitation in rodents (Table 1). Pulsed stimulation with high irradiances, frequencies or pulse lengths causes temperature increases of almost 1 °C at equilibrium, potentially leading to changes in cell function and viability [36]. This illustrates the importance of a case dependent study of temperature evolution during optical stimulation, with knowledge of the optical and thermal properties of the specific tissue. The temperature model described here suffices in applications where the calculation of the upper limit of the temperature change is relevant in order to assess potential heat-induced damage. However, for applications where accurate temperature deposition into the tissue needs to be known, one should take into account diffusion during light absorption [35], and spatial information such as blood flow should be added to take into account cooling and temperature gradients.

4. Conclusions

We measured the absorption and reduced scattering coefficients of multiple regions in the brain, over a

continuous spectrum between 470 nm and 1040 nm, using contact spatially resolved spectroscopy. In general, absorption has a maximum at 560 nm, due to hemoglobin molecules, and the reduced scattering coefficient decreases with increasing wavelength. The cortex, hippocampus, and striatum have lower μ_a and μ'_s values compared to the thalamus (Figure 2). This could be explained by the fact that the internal capsule contributes to an increase in estimated absorption and reduced scattering coefficients of the thalamus.

A relatively large spread was observed for optical properties measured in different positions and samples (Figure 1), indicating the high sensitivity of absorption and scattering to tissue composition and structure. Therefore, a dedicated evaluation of each problem is recommended for planning optogenetic experiments. A major advantage of the cSRS method is that it is non-destructive for surface tissues, it has potential to be applied for *in vivo* characterization of cortical tissue. The optical properties of the human and rat cortex in previous literature exhibit significant variations due to the different measurement protocols, a comparative study would be very valuable.

We investigated light irradiance distribution in the brain when different optic fibers are employed for launching light. The results show that for the same input power, fibers with higher NA and core diameter generate broader beam profiles in radial direction, but shorter in the axial direction. Both the irradiance profile and local heating need to be taken into account when choosing a fiber for a specific experiment. Whereas for the same input power, a SM fiber will reach deeper in the tissue, the irradiance at the fiber-tissue surface is approx. 500 times larger when using a SM fiber instead of a MM fiber. Therefore the use of MM fibers (and slightly higher power) is suggested when the targeted cells are far from the fiber tip, minimizing the risk for phototoxic effects and heat damage. For stimulation of cells in the vicinity of the fiber tip, excessive heating is less probable since less power is required and the fiber choice depends on the experimental goal. A MM fiber will stimulate cells in shallow, but wide regions; whereas a SM fiber will stimulate neurons in deep, but narrow regions. Knowledge of the optical coefficients and how external properties affect the irradiance distribution allows one to plan an optogenetic experiment carefully.

The temperature evolution during fiber-optic based pulsed stimulation of neurons was evaluated at the fiber-brain interface for typical optogenetic stimulation protocols described in literature. The results indicate that most of the published protocols do not induce excessive tissue heating. Nevertheless, extra attention should be given to experiments in which opsins with less light sensitivity are used (high activation threshold, low photoconductivity – e.g. Archaerhodopsin). Since the absorption coefficient is low for red light, the use of opsins photoactivatable above 600 nm will have a big advantage of lower phototoxic risk and less heating. Whereas optical properties have been measured in different tissue types *in vitro*, structural changes, temperature differences, and blood drainage will have an impact on those properties. Therefore, a method should be elaborated for *in vivo* characterization of the optical properties.

Author biographies Please see Supporting Information online.

References

[1] O. Yizhar, L. E. Fenno, T. J. Davidson, M. Mogri, and K. Deisseroth, Neuron **71**(1), 9–34 (2011).

[2] R. Pashaie and R. Falk, IEEE Transactions on Bio-Medical Engineering **60**(2), 268–280 (2013).

[3] F. Pisanello, L. Sileo, I. A. Oldenburg, M. Pisanello, L. Martiradonna, J. A. Assad, B. L. Sabatini, and M. De Vittorio, Neuron **82**(6), 1245–1254 (2014).

[4] E. Papagiakoumou, V. de Sars, D. Oron, and V. Emiliani, Optics Express **16**(26), 22039–22047 (2008).

[5] M. Scanziani and M. Häusser, Nature **461**(7266), 930–939 (2009).

[6] N. McAlinden, D. Massoubre, E. Richardson, E. Gu, S. Sakata, M. D. Dawson, and K. Mathieson, Optics Letters **38**(6), 992–994 (2013).

[7] P. Van der Zee, M. Essenpreis, and D. T. Delpy, Proc. SPIE **1888**, 454–465 (1993).

[8] A. N. Yaroslavsky, P. C. Schulze, I. V. Yaroslavky, R. Schober, F. Ulrich, and H. J. Schwarzmaier, Physics in Medicine and Biology **47**(12), 2059–2073 (2002).

[9] M. Mesradi, A. Genoux, V. Cuplov, D. A. Haidar, S. Jan, I. Buvat, and F. Pain, Journal of Biomedical Optics **18**(11), 117010 (2013).

[10] M. Azimipour, R. Baumgartner, Y. Liu, S. L. Jacques, K. Eliceiri, and R. Pashaie, Journal of Biomedical Optics **19**(7), 75001 (2014).

[11] I. Nishidate, K. Yoshida, and M. Sato, Applied Optics **49**(34), 6617–6623 (2010).

[12] J. F. Beek, P. Blokland, P. Posthumus, M. Aalders, J. W. Pickering, H. J. Sterenborg, and M. J. van Gemert,

Physics in Medicine and Biology **42**(11), 2255–2261 (1997).

[13] A. M. Aravanis, L. P. Wang, F. Zhang, L. A. Meltzer, M. Z. Mogri, M. B. Schneider, and K. Deisseroth, Journal of Neural Engineering **4**(3), S143–156 (2007).

[14] M. L. Huff, R. L. Miller, K. Deisseroth, D. E. Moorman, and R. T. LaLumiere, PNAS **110**(9), 3597–3602 (2013).

[15] N. Nguyen Do Trong, A. Rizollo, E. Herremans, M. Vanoli, G. Cortellino, C. Erkinbaev, M. Tsuta, L. Spinelli, D. Contini, A. Torricelli, P. Verboven, J. De Baerdemaeker, B. Nicolai, and W. Saeys, Innovative - Food Science and Emerging Technologies **21**, 160–168 (2014).

[16] R. Watté, N. Nguyen Do Trong, N. Nguyen Do Trong, B. Aernouts, C. Erkinbaev, J. De Baerdemaeker, B. Nicolai, and W. Saeys, Optics Express **21**(23), 32630–32642 (2013).

[17] L. Wang, S. L. Jacques, and L. Zhenb, Computer Methods and Programs in Biomedicine **2607**(713), 131–146 (1995).

[18] S. Prahl, Oregon Medical Laser Centre website, http://omlc.org/software/mc/ (2007)

[19] M. Kohl, U. Lindauer, G. Royl, M. Kuhl, L. Gold, A. Villringer, and U. Dirnagl, Phys. Med. Biol. **45**, 3749–3764 (2000).

[20] M. M. Elwassif, Q. Kong, M. Vazquez, and M. Bikson, Journal of Neural Engineering **3**(4), 306–315 (2006).

[21] M. J. C. Van Gemert, G. W. Lucassen, and A. J. Welch, Physics in Medicine and Biology **41**, 1381–1399 (1996).

[22] F. P. Incropera and D. P. DeWitt, Fundamentals of Heat and Mass Transfer (John Wiley and Sons, 2002).

[23] J. Wells, C. Kao, P. Konrad, T. Milner, J. Kim, A. Mahadevan-Jansen, and E. D. Jansen, Biophysical Journal **93**(7), 2567–2580 (2007).

[24] J. Steinke and P. Shepherd, Clinical Chemistry **38**(7), 1360–1364 (1992).

[25] B. Cletus, R. Kunnemeyer, P. Martinsen, and V. A. McGlone, Journal of Biomedical Optics, **15**(1) (2015).

[26] B. Gysbrechts, N. Nguyen Do Trong, L. Wang, H. Cabral, Z. Navratilova, F. P. Battaglia, W. Saeys, and C. Bartic, Proc. SPIE **9129**, 912–936 (2014).

[27] S. L. Jacques, Physics in Medicine and Biology **58**(11), R37–61 (2013).

[28] Z. Qian and Y. Gu, OSA Chinese Optics Letters **3**, S167–169 (2005).

[29] S. A. Prahl, Optical Absorption of Hemoglobin, omlc. ogi.edu/spectra/hemoglobin/index.html

[30] H. Wang, J. Peca, M. Matsuzaki, K. Matsuzaki, J. Noguchi, L. Qiu, D. Wang, F. Zhang, E. Boyden, K. Deisseroth, H. Kasai, W. C. Hall, G. Feng, and G. J. Augustine, PNAS **104**(19), 8143–8148 (2007).

[31] F. P. Bolin, L. E. Preuss, R. C. Taylor, and R. Ference, Appl. Opt. **28**, 2297–2303 (1989).

[32] T. Gahm and S. Witte, Journal of microscopy **141**, 101–110 (1986).

[33] X. Han, Progress in brain research (1st ed., **Vol. 196**). Elsevier (2012).

[34] I. Ozden, J. Wang, Y. Lu, T. May, J. Lee, W. Goo, D. J. O'shea, P. Kalanithi, I. Diester, M. Diagne, K. Deisseroth, K. Shenoy, and A. V. Nurmikko, Journal of Neuroscience Methods **219**(1), 142–154 (2013).

[35] M. J. Van Gemert and A. J. Welch, Lasers in Surgery and Medicine **9,** 405–421 (1989).

[36] P. Andersen and E. I. Moser, Hippocampus **5**(6), 491–498 (1995).

[37] P. Anikeeva, A. S. Andalman, I. Witten, M. Warden, I. Goshen, L. Grosenick, L. A. Gunaydin, L. M. Frank, and K. Deisseroth, Nature Neuroscience **15**(1), 163–170 (2012).

[38] J. A. Cardin, M. Carlen, K. Meletis, U. Knoblich, F. Zhang, K. Deisseroth, L. H. Tsai, and C. I. Moore, Nature Protocols **5**(2), 247–254 (2010).

[39] J. Wang, F. Wagner, D. A. Borton, J. Zhang, I. Ozden, R. D. Burwell, A. V. Nurmikko, R. van Wagenen, I. Diester, and K. Deisseroth, Journal of Neural Engineering **9**(1), 016001 (2012).